Photographic Text-to-Image Synthesis with a Hierarchically-nested Adversarial Network

Anonymous CVPR submission

Paper ID ****

Abstract

This paper presents a novel method to deal with the challenging task of generating images conditioned on semantic image descriptions. We propose an effective end-to-end single-stream network that can generate photographic high-resolution images (up to 512^2). Our method leverages the deep representations of convolutional layers and introduces accompanying hierarchical-nested adversarial games inside the network hierarchy, which regularize intermediate representations and assist training to capture the complex image statistics. We present an extensile network architecture to cooperate with discriminators and push generated images to high resolutions. We adopt a multi-purpose adversarial learning strategy at multiple nested hierarchical side outputs to encourage more effective image-text alignment in order to guarantee the semantic consistency and image fidelity simultaneously. Furthermore, we introduce a new visual-semantic similarity measure to evaluate the semantic consistency of generated images. With extensive experimental validation on three major datasets, our method significantly improves previous state of the arts on all datasets over different evaluation metrics.

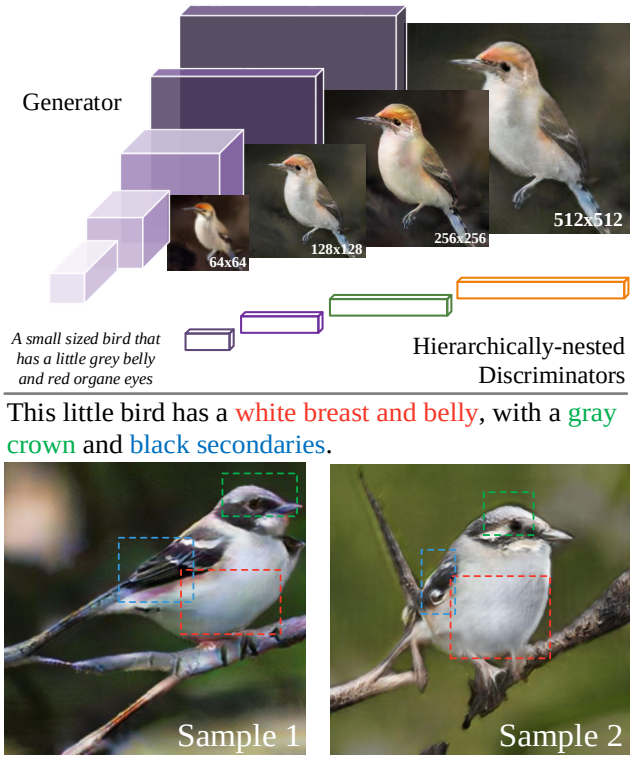

Figure 1: Top: Overview of our hierarchically-nested adversarial network. Bottom: Two fine-grained sample results.

1. Introduction

Photographic text-to-image synthesis is a significant problem in generative model research [34], which aims to learn a translation from a semantic text embedding space to a complex RGB image space. This task requires the generated images to be *semantically consistent*, i.e., the generated images not only preserve sketch concepts in descriptions but also fine-grained descriptive details in image pixels. However, insufficient methods are developed to successfully address this task due to its particular challenges.

Generative adversarial networks (GANs) have become the main solution to this task. Reed *et al*. [34] address this task through a GAN based framework. But this method only handles image up to 64^2 resolution and can barely generate vivid object details. Based on this method, Zhang *et al*. [44] present a successful approach (StackGAN) by stacking another low-to-high resolution GAN to generate high-quality 256^2 images, with two separate stage training. Later on, Dong *et al*. [9] propose to bypass the difficult of translate vector embedding to RGB images and treat it as an pixel-to-pixel translation [16], by re-rendering an arbitrary-style training (128^2) image conditioned on a targeting description. But its high-resolution synthesis ability is unclear. At present, how to train from the low-dimensional text space to synthesize high-resolution and diverse images in an fully end-to-end manner is still an open and attractive question.

We outline several empirical reasons for the challenges

of text-to-image synthesis using GANs. The first is the fundamental difficulty of balancing the convergence between generators and discriminators [12, 37]. The second is stably modeling the huge pixel space in high-resolution images [44]. An effective strategy to regularize generators is critical to help capture the complex image statistics [14] as well as guarantee semantic consistency. With careful consideration of these problems, in this paper, we propose a novel end-to-end method that can directly model high-resolution image statistics and generate semantically consistent and photographic image (see Figure 1). The contributions are described as follows.

Our generator resembles a simple vanilla-like GAN, without requiring any internal text conditioning like [44] or outside image annotation supervision like [7]. To tackle the problem of the big leap from the text space to the high-resolution image space, our insight is to leverage and regularize hierarchical representations with additional deep adversarial constraints. We introduce accompanying hierarchically-nested objectives at multi-scale intermediate layers to play adversarial games and thereby encourage the generator approaching the real training data distribution. We also propose a novel convolutional neural network (CNN) framework for the generator to cooperate with our nested discriminators more effectively. To guarantee the image diversity and semantic consistency, we enforce nested discriminators at different hierarchies to simultaneously differentiate real-and-fake image-text pairs as well as real-and-fake global images or local image patches with certain focal ranges. This multi-purpose conditional adversary is mutually beneficial to allow each focus on its respect duty.

We validate our proposed method on three datasets, CUB birds [41], Oxford-102 flowers [30], and large-scale MSCOCO [24]. In complement of the image diversity evaluation metric (inception score [37]), we introduce a new visual-semantic similarity measurement to evaluate th alignment between generated images and corresponded text. Extensive experimental results and analysis demonstrate the effectiveness of our method and significantly improved performance compared against previous state of the arts on three metrics. All source code will be released.

2. Related Work

We discussed related work and further clarify the novelty of our method by comparing with them.

Deep generative models attract wide interests recently, including GANs [12], Variational Auto-encoders (VAE) [19], etc [32]. There are substantial existing methods investigating better usage of GANs for different applications, such as image synthesis [33, 38], (unpaired) pixel-to-pixel translation [16, 46], medical applications [6], etc [22, 14].

Text-to-image synthesis not only requires diverse and high-quality generation but also requires precise semantically consistent mapping in the image space. Reed *et al*. [34] is th first to introduce a method that can generate 64^2 resolution images, which is similar with DCGAN [33]. This method presents a new strategy for image-text matching aware adversarial training. Reed *et al*. [35] propose generative adversarial what-where network (GAWWN) to enable location and content instructions in text-to-image synthesis, which uses extra information to help generate 128^2 resolution images. StackGAN *et al*. [44] propose a two-stage stacking GAN training approach that is able to generate 256^2 compelling results. Recently, Dong *et al*. [9] propose to learn a joint embedding of images and text so as to re-render a prototype image conditioned on a targeting description. Cha *et al*. [28] explore the usage of the perceptional loss with a CNN pretrained on ImageNet [17] and Dash *et al*. [7] make use of auxiliary classifiers (similar with [31]) to assist GAN training for text-to-image synthesis.

Learning a continuous mapping from low-dimensional embeddings to a complex real data distribution is a long-standing problem. Although GANs have made significant progress, there are still many unsolved difficulties, e.g. training instability and high-resolution extensions. Wide methods have been proposed to address those tasks, through various stabilization training techniques [36, 1, 3, 38, 31], regularization using outside knowledge (e.g. image labels, ImageNet CNNs, etc) [10, 22, 7, 7], or multiple discriminators [27, 11, 43]. *While our method does not use any extra information apart from training paired text and images.* Moreover, it is easy to see the training difficulty increases significantly as targeting image resolution increases.

To synthesize high-resolution images, cascade networks are useful to decompose original difficult tasks to multiple subtasks (Figure 2 A). Denton *et al*. [8] train a cascade of GANs within a Laplacian pyramid framework (LAPGAN) and use each to generate difference images, conditioned on random noises and the output from the last pyramid level, and thereby push up the output resolution through by-stage refinement. StackGAN also shares similar strategy with LAPGAN. Following this strategy, Chen *et al*. [5] present a cascaded refinement network to synthesize high-resolution scene from semantic maps. Huang *et al*. [14] propose a top-down stacked GAN to leverage mid-level representations, which shares some similarities with StackGAN and our method. However, this method needs multiple symmetric bottom-up pre-trained discriminators and the usage for high-resolution image is unclear. Recently, Karras *et al*. [18] propose a progressive training of GANs for very high-resolution image generation (Figure 2 C). *Compared with these strategies that train low-to-high resolution GANs progressively, our method has advantages of leveraging multi-level representations to encourage implicit subtask integration, which makes end-to-end high-resolution image synthesis in a single vanilla-like GAN possible.*

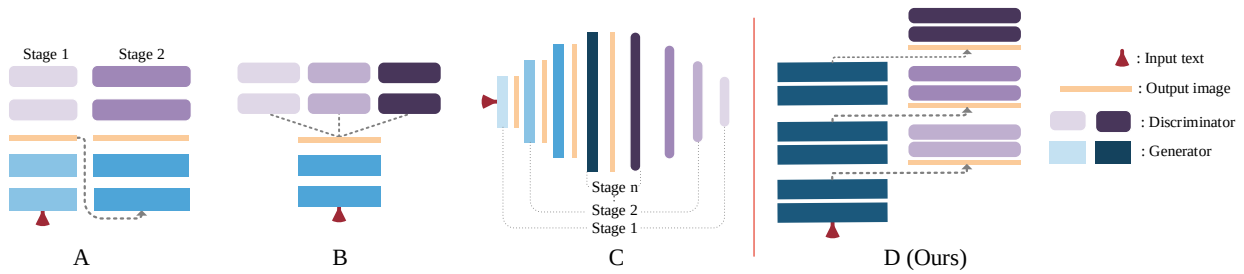

Figure 2: Overviews of some typical GAN frameworks. **A** decomposes tasks multi-stage GANs [44, 8]. **B** uses multiple discriminators with one generator [11, 29]. **C** progressively trains symmetric discriminators and generators [18, 14]. **A** and **C** can be viewed as decomposing high-resolution tasks to multi-stage low-to-high resolution tasks. **D** is our proposed framework that uses a single-stream generator with hierarchically-nested discriminators trained end-to-end.

Leveraging hierarchical representations of neural networks is an effective way to enhance implicit multi-scaling and ensembling for tasks such as image recognition [23] and pixel or object classification [42, 4, 26]. DSN [23] proposes deep supervision in hierarchical convolutional layers to increase the discriminativeness of feature representations. *Our hierarchically-nested adversarial objective is inspired by these kinds of CNNs with deep supervision.*

3. Method

3.1. Adversarial objective basics

In brief, the two-player game in GANs [12] is played by a generator G network and a discriminator D network, which are alternatively trained to compete with each other and thereby improve each other. The discriminator is optimized to distinguish synthesized images from real images, meanwhile, the generator is trained to generate realistic images to fool the discriminator. Concretely, the overall min-max optimization objective is defined as:

$$G^*, D^* = \arg \min_G \max_D \mathcal{L}(D, G) \tag{1}$$

where the loss $\mathcal{L}$ aims to minimize the Jensen-Shannon divergence between the data and model distributions.

3.2. Hierarchical-nested adversarial objectives

Numerous methods have demonstrated a variety of ways to build GANs for image synthesis. Figure 2 and Section 2 discuss some typical frameworks. Our method explores a new dimension of playing this adversarial game along the depth of a CNN (Figure 2 D), which integrates additional discriminators at mid-level features of the generator $\mathcal{G}$. The hierarchically-nested objectives act as regularizers to the hidden space of $\mathcal{G}$, which can reduce the training instability and also offer a short path for better error signals.

The proposed $\mathcal{G}$ is a network (see Section 3.4), with $s-1$ side outputs at the intermediate layers:

$$X_1, ..., X_s = \mathcal{G}(\boldsymbol{t}, \boldsymbol{z}), \tag{2}$$

where $\boldsymbol{z} \sim \mathcal{N}(0, 1)$ denotes a random noise and $\boldsymbol{t} \sim p(data)$ denotes a sentence embedding vector in the real training data distribution (generated by a text character encoder). $\mathcal{G}$ produces $s-1$ side outputs (size-growing images) and a final output X_s with the highest resolution.

For each side output X_i, we propose to apply a discriminator D_i to perform independently adversarial games. Therefore, our full min-max objective can be defined as follows:

$$\begin{gathered} \mathcal{G}^*, \mathcal{D}^* = \arg \min_G \max_{\mathcal{D}} \mathcal{L}(\mathcal{G}, \mathcal{D}, \mathcal{Y}, \boldsymbol{t}, \boldsymbol{z}) \\ \text{where } \mathcal{D} \in \{D_1, ..., D_s\},\ \mathcal{Y} = \{Y_1, ..., Y_s\} \end{gathered} \tag{3}$$

where $\mathcal{Y}$ denotes training images at multi-scales, $\{1, ..., s\}$. Compared with Eq. (1), one generator competes with multiple discriminators at different hierarchies. Discriminators do not share weights with each other, which offers them full flexibility to focus on learning diverse discriminative features in different contextual scales. In principle, the lower-resolution side output is forced to learn semantic consistent image structures (e.g., object sketch, color, and background), and the subsequent higher-resolution side outputs are used to render details to the images. Since the model is trained in an end-to-end fashion, we can observe more consistent information exhibited in both lower and higher-resolution outputs than StackGAN [44]. More results can be founded in experiments. According to this goal, we present the following adversarial losses to support more effective multi-purpose discriminators.

3.3. Functional adversarial losses

Our generator produces size-growing side outputs which compose an image pyramid. We leverage the hierarchy of it and allow adversarial losses to be multi-purpose to guarantee both semantic consistency and image fidelity.

To guarantee semantic consistency, we adopt the matching-aware pair loss proposed by [34]. The discriminator is designed to take image-text pairs as inputs and is

trained to identify two types of fakes: real image with mismatched text and fake image with conditioned text.

The pair loss is designed to capture the global semantic context. However, this loss has two major weaknesses. First, there is no explicit loss that force the discriminator to differentiate real images from fake images. Second, as the image resolution goes higher, it might be challenging for a global pair-loss discriminator to capture local fine-grained details. In addition, as pointed in [38], a single global discriminator may over-emphasize certain unexpected image features and lead to artifacts.

To guarantee image fidelity and overcome these two weaknesses, our solution is to add local adversarial image losses on image patches. The insights are two folds:

- Further forcing the generated samples to have only only global but also local similar statistics to real image patches, which is beneficial for rendering fine-grained details.
- Image loss without using paired text can be beneficial in the sense that it focus more on image information. The richness of discriminator supervision usually has advantages for generalization.

We expect the low-resolution discriminator to focus on global structures, while high-resolution outputs focus more on local image details. Therefore, through the pyramid of the size-growing side outputs, we configure the focal range (the size of each non-overlapping image patch need to classify) to be also growing. The local image adversarial loss is implemented as a fully CNN [38, 46]. Figure 3 illustrates how hierarchically-nested discriminators measure the two losses on the generated images.

Full Objective Overall, our hierarchically-nested discriminators $\{D_i\}$ minimize the following objective[1]:

$$\mathcal{L}(\mathcal{G},\mathcal{D}) = \sum_{i=1}^{s}\Big(L_2\big(D_i(Y_i)\big) + L_2\big(D_i(Y_i,\boldsymbol{t}_Y)\big) + \overline{L_2}\big(D_i(X_i)\big) + \overline{L_2}\big(D_i(X_i,\boldsymbol{t}_{X_i})\big) + \overline{L_2}\big(D_i(Y_i,\boldsymbol{t}_{\overline{Y}})\big)\Big) \tag{4}$$

where $X_i = \mathcal{G}(\boldsymbol{t}_X, \boldsymbol{z})$. $L_2(x) = (x-\mathbb{I})^2$ is the mean-square loss (we do not use the original cross-entropy loss) and $\overline{L_2}(x) = (x)^2$. For adaptive local image loss with varying focal range, the shape of $x, \mathbb{I} \in \mathbb{R}^{R\times R}$ varies accordingly (see Figure 3) for the local image loss. $R = 1$ refers to the (largest local) global range, e.g., $R \equiv 1$ for the matching aware pair loss. For the matching-aware pair loss, $\{Y_i, \boldsymbol{t}_Y\}$ denotes a matched image-text pair and $\{Y_i, \boldsymbol{t}_{\overline{Y}}\}$ denotes a mismatched image-text pair.

Furthermore, this separation of the image loss from the matching loss in our method opens further possibilities, such as utilizing the unlabeled image to improve both the generator and discriminator. In the spirit of variational auto-encoder [20] and the practice of [44], namely conditional augmentation (CA), we sample the input text variable $\boldsymbol{t}$ from a Ganssian distribution $\mathcal{N}(\mu(\boldsymbol{t}), \Sigma(\boldsymbol{t}))$, where μ and Σ are functions of $\boldsymbol{t}$, which produces a 256-d text input used as the input of the generator. We add the Kullback-Leibler divergence regularization term, $D_{KL}(\mathcal{N}(\mu(\boldsymbol{t}), \Sigma(\boldsymbol{t}))||\mathcal{N}(0, \boldsymbol{I}))$ [20], to the G loss to force the smooth sampling over the text embedding distribution.

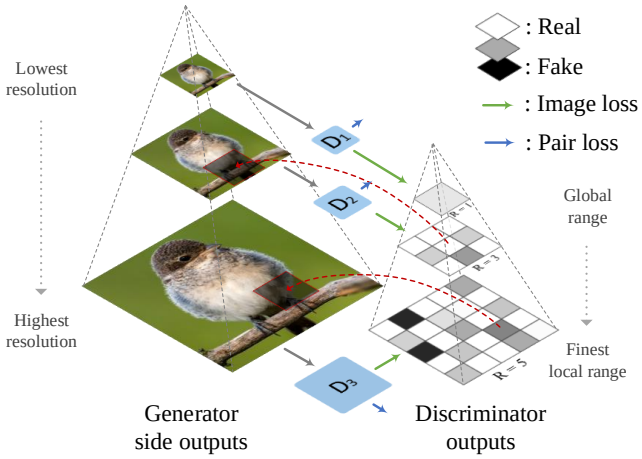

Figure 3: Given an image in the side output pyramid of the generator, the corresponding discriminator D_i computes the matching-aware pair loss and adaptive local image loss (outputting a $R\times R$ probability map to indicate real or fake patches). The focal range increases as image resize grows. Lower range results in finer results.

3.4. Architecture Design

Generator The generator is simply composed by three kinds of modules, termed as K-repeat res-blocks, stretching layers, and linear compression layers. A single res-block in the K-repeat res-block is a modified[2] residual block [13], which contains two convolutional (conv) layers (with batch normalization (BN) [15] and ReLU). The stretching layer serves to reduce feature map size and dimension. It simply contains an scale-2 nearest up-sampling layer followed by a convolutional layer with BN+ReLU. The linear compression layer is one conv layer followed by a Tanh to directly compress features map to the RGB space (as side outputs) linearly. We prevent any non-linear functions that could impede the gradient signals. Starting from a $1024\times4\times4$ embedding, which are computed by the CA output followed by a trainable embedding matrix, the generator simples use M K-repeat res-blocks connected by $M-1$ in-between stretching layers until the feature maps reach to the targeting

[1]The objective of the generator is omitted as it can be easily inferred.

[2]We remove ReLU after the skip-addition of each residual block, with an intention to reduce sparse gradients.

resolution. So for 256×256 resolution with K=1, there are M=6 1-repeat res-blocks and 5 stretching layers. With a predefined side-output scales $\{1, ..., s\}$, we apply the compression layer at those scales to produce synthetic images (i.e., side outputs).

Discriminator The discriminator simply contains consecutive stride-2 conv layers with BN and LeakyReLU. There are two branches are added on the upper layer for the proposed functional discriminator design (see next section). One branch is a direct fully convolutional layers to produce a $R \times R$ probability map (see Figure 3) and classify each location as real or fake. Another branch first concatenates a 128×4×4 text embedding (replicated by a reduced 128-d text embedding). Then we use an 1×1 conv to fuse text and image information and a 4×4 conv layer to classify the image-text pair is real or fake.

All other intermediate conv layers for both generators and discriminators use 3×3 kernels (with reflection padding). We also experimented other normalization (i.e. instance normalization [40] and layer normalization [2]) used by recent advances [46, 5]. Both are not satisfactory.

3.5. Training Details

The Adam optimizer is used for all experiments. The initial learning rate is set as 0.0002 and decreased by half for every 100 epochs (30 for COCO). The CUB and Oxford-102 datasets are trained for 500 epochs in total (250 epochs for COCO). For the adaptive local image loss, we set $R = 1$ for 64^2 side output, $R = 3$ for 128^2 side output and $R = 5$ for 256^2 and 512^2 outputs. We use 1-repeat residual block for the generator till 256^2 resolution. To generate 512^2 images, we pre-train the generator to 256^2 due to the limitation of GPU memory. We use 3-repeat res-block followed by the stretching and linear compression layer. maybe delete the l1 loss description. Since the 256^2 image already captures the overall semantics and details, to encourage the 512^2 maintain these information, we also use a reconstruction loss to self-regularize the generator in case the discriminator confuses the expected output.

4. Experiments

This section evaluates the proposed method both qualitatively and quantitatively on three public datasets. We denote our method as **HDGAN**, referring as High-Definition results and the idea of Hierarchically-nested Discriminators.

Dataset We test on three widely used datasets. The CUB dataset [41] contains 11,788 bird images belonging to 200 different categories. We pre-process and split the images following the same pipeline in [34, 44] The Oxford-102 dataset [30] contains 8189 flow images in 102 different categories. Each image in both datasets is associated with 10 text descriptions. In the COCO dataset, [24] there are 80k training images and a validation 40k images. Each image has 5 text descriptions. We use the pre-trained text encoder model provided in [34] to encode each text description into a 1024 embedding vector.

Method	Dataset		
	CUB	Oxford	COCO
GAN-INT-CLS	2.88±.04	2.66±.03	7.88±.07
GAWWN	3.60±.07	-	-
StackGAN	3.70±.04	3.20±.01	8.45±.03*
StackGAN++	3.84±.06	-	-
TAC-GAN	-	3.45±.05	-
HDGAN	**4.15±.05**	**3.45±.07**	**11.29±.18**

*Recently, it updated to 10.62±.19 in its source code.

Table 1: The inception-score evaluation on three datasets. The higher score reflects more meaningful synthetic images and higher diversity. The proposed HDGAN outperforms others significantly.

Evaluation metric We use three different quantitative metrics to evaluate our method. 1) Inception score [37] is a measurement of both objectiveness and diversity of generated images, it is closely correlated with human judgment on the image quality. For CUB and oxford-102, we use the fine-tuned inception model provided by StackGAN. For MS COCO dataset, we directly use the model pre-trained on ImageNet. 2) We also adopt the multi-scale structural similarity (MS-SSIM) metric [37] for further validation. It tests the variation of generated outputs and can find mode collapses reliably [31]. Lower score indicates higher variance. 3) Visual-semantic similarity.

Visual-semantic similarity Since the aforementioned evaluation methods can not measure alignment between the generated images and the text description, we introduce a new qualitative measurement, namely visual-semantic similarity (VS similarity) [21]. Denote $\boldsymbol{v}$ as the feature vector extract by a pre-trained CNN model f_{cnn} (inception v2[39] pre-trained on Imagenet), and $\boldsymbol{t}$ denote the text embedding. We define a scoring function $s(\boldsymbol{x}, \boldsymbol{y}) = \frac{\boldsymbol{x} \cdot \boldsymbol{y}}{||\boldsymbol{x}|| \cdot ||\boldsymbol{y}||}$. We learn two mapping functions f_v and f_t, which map both image and sentence embeddings into one semantic space $\mathbb{R}^{512}$, by minimizing the following bi-directional ranking loss:

$$\begin{aligned} \mathcal{L}_{vs} = & \sum_{\boldsymbol{v}} \sum_{\boldsymbol{t}^-} \max(0, \delta - s(f_v(\boldsymbol{v}), f_t(\boldsymbol{t}^-))) \\ & + \sum_{\boldsymbol{t}} \sum_{\boldsymbol{v}-} \max(0, \delta - s(f_t(\boldsymbol{t}), f_v(\boldsymbol{v}^-))) \end{aligned} \tag{5}$$

where δ is the margin, which is set as 0.2, every $(\boldsymbol{v}, \boldsymbol{t})$ is a ground truth image text pair, $\boldsymbol{t}^-$ denotes a mismatching text description for the image corresponding to $\boldsymbol{v}$, and vice-versa for $\boldsymbol{v}^-$. In the testing stage, given an text embedding $\boldsymbol{t}$, and the generated images o, the corresponding vs-similarity will be calculated as $s(f_{cnn}(o), \boldsymbol{t})$.

Figure 4: The generated images on CUB compared with StackGAN. Each sample shows the input text and generated 64^2 (left) and 256^2 (right) images. Our results have significantly higher quality and preserve more semantic details, for example, "the brown and white feathers and read head" in the last column is much better reflected in our images. Moreover, we observed our birds have more diverse poses (e.g. the frontal view in the the second and the back view forth columns).

Figure 5: The generated images on Oxford compared with StackGAN (second row). Our generated images perform more natural satisfiability and higher contrast.

Method	Dataset		
	CUB	Oxford	COCO
StackGAN	.228±.162	.278±.134	−±−
Ground Truth	.302±.151	.336±.138	-
HDGAN	**.246±.157**	**.296±.131**	-

Table 2: The VS similarity evaluation on three datasets. The higher score represents higher semantic consistency between the generated images and the text information.

4.1. Comparative Results

To validate our method, we compare our results with GAN-INT-CLS [34], GAWWN [35], TAC-GAN [7], StackGAN [44] and also its improved version StackGAN++ [45], and Progressive GAN [18] [3] We especially compare with the current state of the art, StackGAN (results are obtained from its provided model).

Table 1 shows the quantitative inception-score evaluation. We follow StackGAN to sample $30,000$ images for evaluation. HDGAN achieves significantly improvement compared against other methods. For example, it improves StackGAN by .45 and StackGAN++ by .31 on CUB. HDGAN achieves competitive results with TAC-GAN on Oxford. TAC-GAN uses image labels to increase the discriminability of generators, while we do not use any extra knowledge. Figure 4 and Figure 5 show the results compared with StackGAN and strongly demonstrate the superiority of HDGAN. Mover, we also qualitatively test the diversity of samples conditioned on the same text in Figure 6 left. It also demonstrates how well the model learned to cover the input distribution. HDGAN shows obvious more successful samples than StackGAN.

Table 2 shows the qualitative vs-similarity comparison results on three datasets. We also add the evaluation results on the ground truth image and sentence pair for ref-

[3] StackGAN++ and Prog.GAN are two very recently released preprints we noticed. We acknowledge them as they also target at generating high-resolution images, in spite of their differences in motivations and network and training designs from ours.

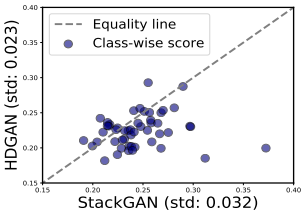

Method	MS-SSMI
StackGAN	0.234
Prog.GAN	0.225
HDGAN	**0.215**

Table 3: Left: Class-wise MS-SSMI evaluation. Lower score indicates higher intraclass invariance. The points below the equality line represent classes our HDGAN wins. Right: Overall (no class-wise) score evaluation.

erence. Our proposed method achieves much better results on both CUB and Oxford datasets. Since we do not have a pre-trained StackGAN model for coco dataset, we omit the comparison. This results demonstrate that HDGAN is better at capturing visual semantic correlation.

Table 3 shows the MS-SSMI image quality evaluation score compared with StackGAN and Prog.GAN on CUB. StackGAN and our HDGAN use the semantic text as input so the generated images retain class information. We compare the score with StackGAN. We randomly sample $20,000$ image pairs (400 per class) and show the class-wise score in the left figure. HDGAN wins in majority of classes and also has lower inter-class standard deviation (.023 vs. .032). Prog.GAN takes noises rather than text. Since MS-SSMI evaluates the image quality without text or class involvement, we can compare with it. Following the procedure of Prog.GAN, we randomly sample $10,000$ image pairs for each comparing method (For Prog.GAN, we use generated 256^2 images provided by the author) and show the results in the right table. Our method outperforms both StackGAN and Prog.GAN.

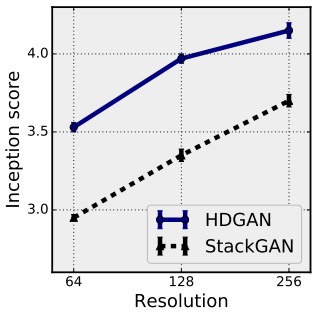

The right figure compares the the multi-resolution inception score on CUB. Our results are from the side outputs of a single model. As can be observed, our 64^2 images outperforms 128^2 images of StackGAN and our 128^2 images outperforms 256^2 images of StackGAN substantially. It strongly demonstrates our HDGAN better preserves semantically consistent information in all resolutions. Figure 6 right shows some testing samples.

4.1.1 Style Transfer Using Sentence Interpolation

Ideally, a trained model should learn a smooth linear latent manifold of the images. To demonstrate our model's generalization capability, we generate images using the linearly interpolated embedding using two source sentences. During this experiment, we fix the all the random noises to make the object and background consistent. As is shown in Figure 7, the generated images show gradual and smooth changes reflecting the semantic changing in sentences, while still maintaining plausible object pose and shape. In the first row, the generated birds gradually turn the color from yellow to red, in the second row, more complicated sentences containing more detailed appearance information (e.g., blue peaks, and yellow wing) are used, we can see that our model is still be able to successfully capture these subtle information and tune the bird appearance gradually.

We also evaluate some sentences that generated by ourself, the resulting images are shown in Figure **??**, as we can see, our model are robust and generalize well to human descriptions that never seen before.

5. On the effects of Individual Components

5.1. Hierarchically-nested adversarial training

Our hierarchically-nested adversarial discriminators a role of regularizing the layer representations (at scale $\{64, 128, 256\}$). In Table **??**, we compare the results by removing part of discriminators. The number of StackGAN emphasizes the importance of using text embeddings with mid-level features of the 256^2 generator by showing an large drop from 3.7 to 3.45 without doing so, which helps maintains the diversity and semantic consistency. While in our method, we only use text embeddings at the input. Our significantly improved results demonstrate that effectiveness of the hierarchically-nested adversarial training to achieve this goal.

5.2. On the Local Image Loss

We also study the effectiveness of the proposed local image loss. We conduct experiments with using architecture with side output 64×64, 128×128 and 256×256 using CUB dataset. As can be seen in Table**??**, we can see that by removing local image loss (denoted as "No Local"), the inception score drop from 4.27 to 3.8. To quantitatively compare the results, we also show generated results using two model in Figure **??**, We can see that, although both models can successfully capture the semantic correspondence between image and sentence, 256×256 results generated by model trained with local image loss provide more local fine-grained details, thus improving the visual quality.

5.3. Design principles

StackGAN shows the difficulty of directly training a vanilla 256×256 GAN to generate meaningful images. We test this extreme case using our method by removing all nested intermediate discriminators (the first row of Table **??**). Our method still generates fairly good results. Figure **??** shows the qualitatively results. Based on our experience,

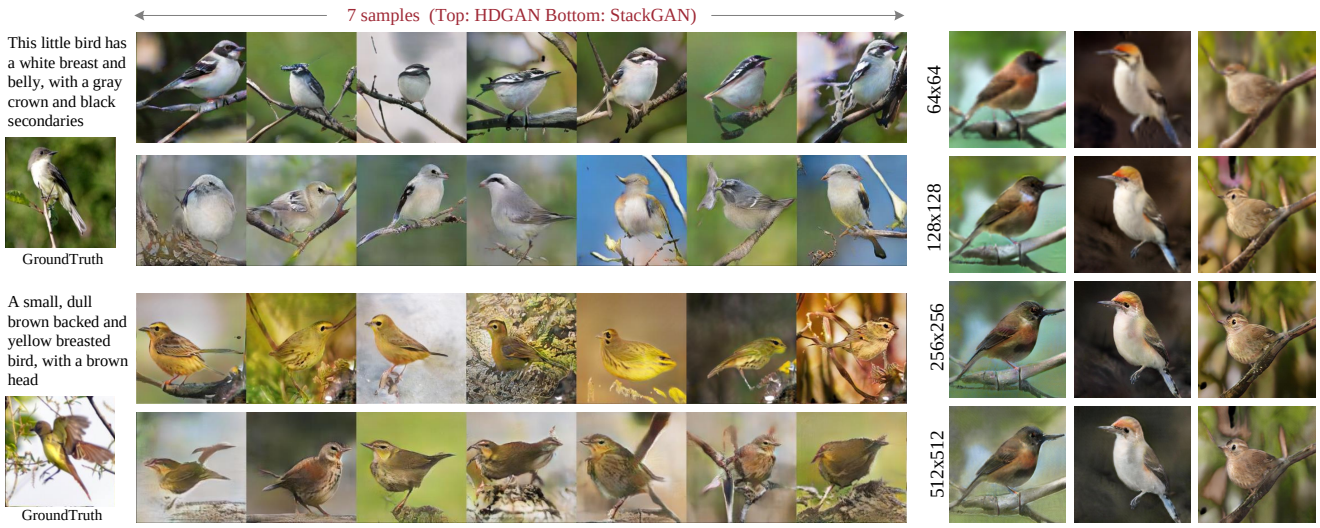

Figure 6: Left: Diversity test given a single input text. Our results show obviously more details and higher diversity. Right: Side outputs of HDGAN with increasing resolutions. Different resolutions are fairly semantically consistent.

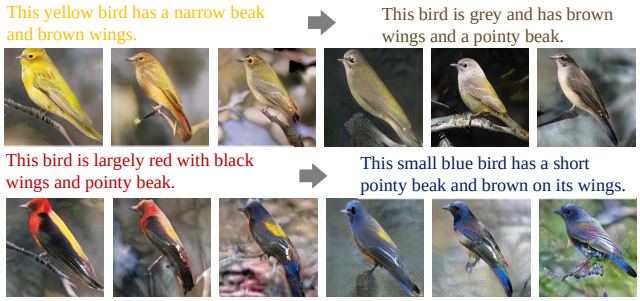

Figure 7: Text interpolation visualization.

Metric	VS	MS-SSMI
w/o Img	.25±.16	.215
w/ global	–	–
w/local	–	–

Components			Score
64	128	256	
		✓	3.52±.04
	✓	✓	3.99±.04
✓		✓	4.14±.03
✓	✓	✓	4.15±.05

Table 4: Ablation study on the local adversarial loss (left) and hierarchically-nested adversarial learning (right). See text for details. See text for details.

the success is because of our framework designs in generators.

Initially, we tried to share top layers of the hierarchical discriminators of HDGAN inspired by [25] with an intuition to reduce their variances and unify their common goal (i.e. differentiates real and fake despite difficult scales). However, we did not find any benefits from this and our independent discriminators can be trained very stably.

6. Conclusion

In this paper, we present a novel and effective method to tackle the problem of generating high resolution images using text description. We introduce the hierarchical nested side outputs for deeply supervising the GAN training. To improve the model's capability to render fine-grained local details, we propose a hierarchal local image loss to boost the training. We also introduce a newly evaluation method for conditional gan, which leverage visual semantic embedding to judge the matching between generated images and provided text description, thus remove the necessary for human evaluation. Extensive experiment results demonstrate that our method work significantly better than existing state of the arts.

References

[1] M. Arjovsky, S. Chintala, and L. Bottou. Wasserstein gan. *arXiv preprint arXiv:1701.07875*, 2017.

[2] J. L. Ba, J. R. Kiros, and G. E. Hinton. Layer normalization. *arXiv preprint arXiv:1607.06450*, 2016.

[3] D. Berthelot, T. Schumm, and L. Metz. Began: Boundary equilibrium generative adversarial networks. *arXiv preprint arXiv:1703.10717*, 2017.

[4] Z. Cai, Q. Fan, R. S. Feris, and N. Vasconcelos. A unified multi-scale deep convolutional neural network for fast object detection. In *ECCV*, pages 354–370. Springer, 2016.

[5] Q. Chen and V. Koltun. Photographic image synthesis with cascaded refinement networks. *ICCV*, 2017.

[6] P. Costa, A. Galdran, M. I. Meyer, M. D. Abràmoff, M. Niemeijer, A. M. Mendonça, and A. Campilho. Towards adversarial retinal image synthesis. *arXiv preprint arXiv:1701.08974*, 2017.

[7] A. Dash, J. C. B. Gamboa, S. Ahmed, M. Z. Afzal, and M. Liwicki. Tac-gan-text conditioned auxiliary clas-

sifier generative adversarial network. *arXiv preprint arXiv:1703.06412*, 2017.

[8] E. L. Denton, S. Chintala, R. Fergus, et al. Deep generative image models using a laplacian pyramid of adversarial networks. In *NIPS*, pages 1486–1494, 2015.

[9] H. Dong, S. Yu, C. Wu, and Y. Guo. Semantic image synthesis via adversarial learning. *ICCV*, 2017.

[10] A. Dosovitskiy and T. Brox. Generating images with perceptual similarity metrics based on deep networks. In *NIPS*, pages 658–666, 2016.

[11] I. Durugkar, I. Gemp, and S. Mahadevan. Generative multi-adversarial networks. *arXiv preprint arXiv:1611.01673*, 2016.

[12] I. Goodfellow, J. Pouget-Abadie, M. Mirza, B. Xu, D. Warde-Farley, S. Ozair, A. Courville, and Y. Bengio. Generative adversarial nets. In *NIPS*, 2014.

[13] K. He, X. Zhang, S. Ren, and J. Sun. Identity mappings in deep residual networks. In *ECCV*, 2016.

[14] X. Huang, Y. Li, O. Poursaeed, J. Hopcroft, and S. Belongie. Stacked generative adversarial networks. *CVPR*, 2017.

[15] S. Ioffe and C. Szegedy. Batch normalization: Accelerating deep network training by reducing internal covariate shift. In *ICML*, 2015.

[16] P. Isola, J.-Y. Zhu, T. Zhou, and A. A. Efros. Image-to-image translation with conditional adversarial networks. *CVPR*, 2017.

[17] J. Johnson, A. Alahi, and L. Fei-Fei. Perceptual losses for real-time style transfer and super-resolution. In *ECCV*, pages 694–711, 2016.

[18] T. Karras, T. Aila, S. Laine, and J. Lehtinen. Progressive growing of gans for improved quality, stability, and variation. In *arXiv preprint arXiv:1710.10196*, 2016.

[19] D. P. Kingma and M. Welling. Auto-encoding variational bayes. *arXiv preprint arXiv:1312.6114*, 2013.

[20] D. P. Kingma and M. Welling. Auto-encoding variational bayes. *CoRR*, abs/1312.6114, 2013.

[21] R. Kiros, R. Salakhutdinov, and R. S. Zemel. Unifying visual-semantic embeddings with multimodal neural language models. *arXiv preprint arXiv:1411.2539*, 2014.

[22] C. Ledig, L. Theis, F. Huszár, J. Caballero, A. Cunningham, A. Acosta, A. Aitken, A. Tejani, J. Totz, Z. Wang, et al. Photo-realistic single image super-resolution using a generative adversarial network. *CVPR*, 2017.

[23] C.-Y. Lee, S. Xie, P. Gallagher, Z. Zhang, and Z. Tu. Deeply-supervised nets. In *Artificial Intelligence and Statistics*, 2015.

[24] T.-Y. Lin, M. Maire, S. Belongie, J. Hays, P. Perona, D. Ramanan, P. Dollár, and C. L. Zitnick. Microsoft coco: Common objects in context. In *ECCV*, 2014.

[25] M.-Y. Liu, T. Breuel, and J. Kautz. Unsupervised image-to-image translation networks. *arXiv preprint arXiv:1703.00848*, 2017.

[26] J. Long, E. Shelhamer, and T. Darrell. Fully convolutional networks for semantic segmentation. In *CVPR*, 2015.

[27] L. Metz, B. Poole, D. Pfau, and J. Sohl-Dickstein. Unrolled generative adversarial networks. *arXiv preprint arXiv:1611.02163*, 2016.

[28] H. T. K. Miriam Cha, Youngjune Gwon. Adversarial nets with perceptual losses for text-to-image synthesis. *arXiv preprint arXiv:1708.09321*, 2017.

[29] T. D. Nguyen, T. Le, H. Vu, and D. Phung. Dual discriminator generative adversarial nets. In *NIPS*, 2017.

[30] M.-E. Nilsback and A. Zisserman. Automated flower classification over a large number of classes. In *ICCVGIP*, 2008.

[31] A. Odena, C. Olah, and J. Shlens. Conditional image synthesis with auxiliary classifier gans. *arXiv preprint arXiv:1610.09585*, 2016.

[32] A. v. d. Oord, N. Kalchbrenner, and K. Kavukcuoglu. Pixel recurrent neural networks. *ICML*, 2016.

[33] A. Radford, L. Metz, and S. Chintala. Unsupervised representation learning with deep convolutional generative adversarial networks. *arXiv preprint arXiv:1511.06434*, 2015.

[34] S. Reed, Z. Akata, X. Yan, L. Logeswaran, B. Schiele, and H. Lee. Generative adversarial text to image synthesis. *ICML*, 2016.

[35] S. E. Reed, Z. Akata, S. Mohan, S. Tenka, B. Schiele, and H. Lee. Learning what and where to draw. In *NIPS*, 2016.

[36] T. Salimans, I. Goodfellow, W. Zaremba, V. Cheung, A. Radford, and X. Chen. Improved techniques for training gans. In *NIPS*, 2016.

[37] T. Salimans, I. Goodfellow, W. Zaremba, V. Cheung, A. Radford, X. Chen, and X. Chen. Improved techniques for training gans. In *NIPS*. 2016.

[38] A. Shrivastava, T. Pfister, O. Tuzel, J. Susskind, W. Wang, and R. Webb. Learning from simulated and unsupervised images through adversarial training. *CVPR*, 2017.

[39] C. Szegedy, W. Liu, Y. Jia, P. Sermanet, S. Reed, D. Anguelov, D. Erhan, V. Vanhoucke, and A. Rabinovich. Going deeper with convolutions. In *CVPR*, June 2015.

[40] D. Ulyanov, A. Vedaldi, and V. Lempitsky. Instance normalization: The missing ingredient for fast stylization. *arXiv preprint arXiv:1607.08022*, 2016.

[41] P. Welinder, S. Branson, T. Mita, C. Wah, F. Schroff, S. Belongie, and P. Perona. Caltech-ucsd birds 200. 2010.

[42] S. Xie and Z. Tu. Holistically-nested edge detection. In *ICCV*, 2015.

[43] J. Yang, A. Kannan, D. Batra, and D. Parikh. Lr-gan: Layered recursive generative adversarial networks for image generation. *arXiv preprint arXiv:1703.01560*, 2017.

[44] H. Zhang, T. Xu, H. Li, S. Zhang, X. Wang, X. Huang, and D. Metaxas. Stackgan: Text to photo-realistic image synthesis with stacked generative adversarial networks. In *ICCV*, 2017.

[45] H. Zhang, T. Xu, H. Li, S. Zhang, X. Wang, X. Huang, and D. Metaxas. Stackgan++: Text to photo-realistic image synthesis with stacked generative adversarial networks. In *arXiv preprint arXiv:1710.10916*, 2017.

[46] J.-Y. Zhu, T. Park, P. Isola, and A. A. Efros. Unpaired image-to-image translation using cycle-consistent adversarial networks. *ICCV*, 2017.